Available online at www.sciencedirect.com
SCIENCE DIRECT®
International Journal of Heat and Mass Transfer 47 (2004) 5365–5373
International Journal of HEAT and MASS TRANSFER
www.elsevier.com/locate/ijhmt

Axisymmetric thermocapillary convection in open cylindrical annuli with deforming interfaces

Bok-Cheol Sim [a], Woo-Seung Kim [a,*], Abdelfattah Zebib [b]

[a] Department of Mechanical Engineering, Hanyang University, Sa 1-Dong, Ansan-si, Kyunggi-Do 425-791, Korea
[b] Department of Mechanical and Aerospace Engineering, Rutgers University, Piscataway, New Jersey 08854-8058, USA

Received 24 April 2003; received in revised form 9 November 2003

Abstract

Two-dimensional thermocapillary convection in an open cylindrical annulus heated from the inside wall is computed. The deformable free surface is obtained as a solution of the coupled transport equations, assuming pinned contact points, at Prandtl number of 30 and prescribed geometry. Only steady convection is possible at any Reynolds number (Re) in the axisymmetric computations with either nondeformable or deformable surfaces. Dynamic free-surface deformations do not induce transitions to oscillatory convection even at large Re and capillary numbers (Ca). Free surfaces are convex near the cold wall stagnation point and concave near the hot wall. Two peaks appear at the free surface at low Re while four peaks are possible at larger Re. Free surface shapes and convection in the interior are insensitive to variations in Ca while the magnitudes of surface ripples increase with Ca. At $Ca = 0$ convection is calculated assuming nondeformable concave surfaces as function of the liquid volume (V) and the contact angle (θ) at the inner boundary. At constant V, peaks of surface velocity increase while central surface temperatures decrease with increasing θ. Curvature significantly influences convection which is more vigorous with increasing V/θ at constant θ/V.

1. Introduction

Buoyant and thermocapillary forces cause convection in the melt during crystal growth on Earth. However, in a microgravity environment, thermocapillary forces dominate. Thus understanding thermocapillary flows is important to material processing in space. Accordingly, there have been a large number of experimental and numerical studies of surface tension driven convection in open rectangular and cylindrical containers. Most of the numerical studies considered thermocapillary convection with nondeformable surfaces, and a few included deformable surfaces.

Schwabe et al. [1] studied experimentally thermocapillary flows with $Pr = 17$ in two types of shallow liquid layers heated from the side: one is a rectangular configuration, the other an annular slot. In the annular slot heated from the inner rod, they observed azimuthal wavetrains travelling on the free surface, and found that the number of wavetrains increased as Ma increased. For thin annular gaps, Schwabe [2] confirmed the existence of azimuthally travelling wavetrains on the free surface. Kamotani et al. [3] investigated experimentally surface tension driven convection with 2 cSt silicone oils induced by placing a cylindrical heater at the center of annuli. Their experiments included flat and curved surfaces, which were determined by the liquid volume.

* Corresponding author. Tel.: +82 31 400 5248; fax: +82 31 418 0153.
E-mail address: wskim@hanyang.ac.kr (W.-S. Kim).

0017-9310/$ - see front matter © 2004 Elsevier Ltd. All rights reserved.
doi:10.1016/j.ijheatmasstransfer.2004.03.031

Nomenclature

Ar	aspect ratio, R/H	u	nondimensional radial velocity
Bi	Biot number, hH/k	V	nondimensional liquid volume
Ca	Capillary number, $\frac{\gamma\Delta T}{\sigma_0}$	$\mathbf{v}$	nondimensional velocity vector
H	height of the cylinder	v	nondimensional axial velocity
h	convective heat transfer coefficient	z	axial or vertical direction
k	thermal conductivity		
Ma	Marangoni number, $Pr \cdot Re$	*Greek symbols*	
P	nondimensional pressure	ν	kinematic viscosity
Pr	Prandtl number, $\frac{\nu}{\alpha}$	μ	dynamic viscosity
R	outer radius of the annulus	α	thermal diffusivity
R_i	inner radius of the annulus	γ	$-\partial\sigma/\partial T$
r	radial direction	σ	surface tension
Re	Reynolds number, $\gamma\frac{\Delta TH}{\nu\mu}$	ρ	density
Re_c	critical Re	θ	contact angle in the inside wall
T	nondimensional temperature		
T^*_{hot}	dimensional inside wall temperature	*Subscript*	
T^*_{cold}	dimensional outside wall temperature	0	reference state
ΔT	characteristic T, $T^*_{hot} - T^*_{cold}$		

Several numerical studies with curved surfaces have been performed in two-dimensional rectangular cavities. Chen et al. [4], Chen and Hwu [5], Hamed and Floryan [6] and Jiang et al. [7] considered oscillatory thermocapillary convection with deformable surfaces in two-dimensional cavities. Two-dimensional numerical simulations of steady convection with deforming surfaces in cavities were studied by Mundrane et al. [8]. Mundrane and Zebib [9] showed that small free surface deformations did not induce transition from steady to oscillatory convection in a two-dimensional cavity with a low Pr fluid. Dynamic surface deformation in liquid bridges were investigated in the limit of small capillary number [10]. Sim et al. [11] performed axisymmetric numerical simulations in liquid bridges with dynamic free surfaces and showed that dynamic surface deformation with $Ca \leqslant 0.1$ was negligible in axisymmetric liquid bridge. Lappa et al. [12,13] showed transition to steady nonaxisymmetric states with low Pr in nondeformable and noncylindrical liquid bridges. Two- and three-dimensional thermocapillary convection with nondeformable curved surfaces were performed in open cylinders and liquid bridges with high Pr by Sim and Zebib [14,15]. They showed that only steady thermocapillary convection with either flat or curved surfaces was possible in strictly axisymmetric computations.

Although a few numerical studies with deformable surfaces have been performed in two-dimensional rectangular cavities, there is no work available for cylindrical annuli. In the present work we report on simulations of two-dimensional thermocapillary convection in open annuli with deformable interfaces. The shape of the free surface is unknown and is calculated as the part of the complete solution. Numerical results with a nondeformable flat surface are compared with those from available space experiments. The influence of Re, Ca, V, and surface heat loss on convection is investigated.

2. Mathematical model

The physical system considered is an open cylindrical annulus with inner and outer radii, $R_i = 0.1R$ and R, as shown in Fig. 1. It is filled with an incompressible, Newtonian fluid to a height H. The aspect ratio ($Ar = R/H$) of 1 and Prandtl number of 30 are used to study the effect of the surface deformation on thermocapillary

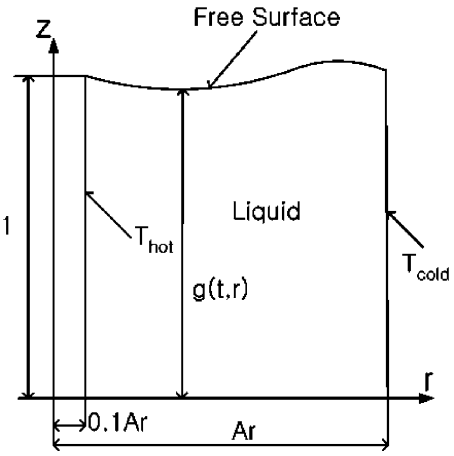

Fig. 1. Physical system.

convection. The vertical inside and outside walls have nondimensional temperatures, $T_{hot} = 1$ and $T_{cold} = 0$, and the bottom is an adiabatic solid wall. Surface tension is assumed a linear function of temperature,

$$\sigma = \sigma_0 - \gamma(T - T_0). \tag{1}$$

With negligible body forces, the nondimensional governing equations are:

$$\nabla \cdot \mathbf{v} = 0, \tag{2}$$

$$Re\left(\frac{\partial \mathbf{v}}{\partial t} + \nabla \cdot (\mathbf{vv})\right) = -\nabla P + \nabla^2 \mathbf{v}, \tag{3}$$

$$Ma\left(\frac{\partial T}{\partial t} + \nabla \cdot (\mathbf{v}T)\right) = \nabla^2 T. \tag{4}$$

The length, temperature, velocity, pressure, and time are normalized with respect to H, ΔT, $\frac{\gamma \Delta T}{\mu}$, $\frac{\gamma \Delta T}{H}$, and $\frac{\mu H}{\gamma \Delta T}$, respectively.

The boundary conditions considered are:

$$u = 0, \quad v = 0, \quad T = 1, \quad \text{at } r = 0.1, \tag{5}$$

$$u = 0, \quad v = 0, \quad T = 0, \quad \text{at } r = 1, \tag{6}$$

$$u = 0, \quad v = 0, \quad \frac{\partial T}{\partial z} = 0, \quad \text{at } z = 0. \tag{7}$$

The nondimensionalized position of the free surface is described by a function $g(t,r)$. Thermal, kinematic and tangential and normal stress balance boundary conditions at the interface are

$$\frac{1}{N}\left(-g'\frac{\partial T}{\partial r} + \frac{\partial T}{\partial z}\right) = BiT, \tag{8}$$

$$v = \frac{\partial g}{\partial t} + g'u, \tag{9}$$

$$(1 - g'^2)\left(\frac{\partial u}{\partial z} + \frac{\partial v}{\partial r}\right) + 2g'\left(\frac{\partial v}{\partial z} - \frac{\partial u}{\partial r}\right) = -N\left(\frac{\partial T}{\partial r} + g'\frac{\partial T}{\partial z}\right), \tag{10}$$

$$-P + \frac{2}{N^2}\left[\frac{\partial v}{\partial z} + g'^2\frac{\partial u}{\partial r} - g'\left(\frac{\partial v}{\partial r} + \frac{\partial u}{\partial z}\right)\right] = \frac{1 - CaT}{CaN}\left(\frac{g''}{N^2} + \frac{g'}{r}\right), \tag{11}$$

where $N = (1 + g'^2)^{1/2}$ and $g' = \frac{\partial g}{\partial r}$. Ca provides a measure of surface deflection in response to thermocapillary-induced stresses. If $Ca = 0$ (large surface tension), the dynamic surface deformations can be neglected and the free surface is nondeformable. The Biot number in Eq. (8) is given by $Bi = hH/k$ where h is a heat transfer coefficient to the surroundings at the cold wall temperature. Free-surface curvature is determined by both surface pressure and normal viscous stresses as shown in Eq. (11).

The initial and boundary conditions for Eq. (11) considered here are:

$$g(t = 0, r) = 1,$$

$$g(t, r = 0.1) = 1,$$

$$g(t, r = 1) = 1. \tag{12}$$

The liquid volume must satisfy the mass conservation, and its total volume should be constant:

$$V = \frac{2\int_{0.1}^{1} rg\,dr}{0.99}, \tag{13}$$

where the nondimensional liquid volume, V, is normalized with respect to $0.99\pi HR^2$.

3. Numerical aspects

In order to solve the problem with a deformable surface, the equations are transformed from the physical domain (t,r,z) into a rectangular computational domain (t,ξ,η).

$$\xi = r \tag{14}$$

$$\eta = z/g(t,r) \tag{15}$$

The transformed governing equations are

$$\frac{1}{\xi}\frac{\partial \xi u}{\partial \xi} - \eta\frac{g'}{g}\frac{\partial u}{\partial \eta} + \frac{1}{g}\frac{\partial v}{\partial \eta} = 0, \tag{16}$$

$$Re\left[\frac{\partial u}{\partial t} - \frac{\eta}{g}\frac{\partial g}{\partial t}\frac{\partial u}{\partial \eta} + \frac{1}{\xi}\frac{\partial \xi u^2}{\partial \xi} - \eta\frac{g'}{g}\frac{\partial u^2}{\partial \eta} + \frac{1}{g}\frac{\partial uv}{\partial \eta}\right] = -\frac{\partial p}{\partial \xi} + \eta\frac{g'}{g}\frac{\partial P}{\partial \eta} - \frac{u}{\xi^2} + \nabla^2 u, \tag{17}$$

$$Re\left[\frac{\partial v}{\partial t} - \frac{\eta}{g}\frac{\partial g}{\partial t}\frac{\partial v}{\partial \eta} + \frac{1}{\xi}\frac{\partial \xi uv}{\partial \xi} - \eta\frac{g'}{g}\frac{\partial uv}{\partial \eta} + \frac{1}{g}\frac{\partial v^2}{\partial \eta}\right] = -\frac{1}{g}\frac{\partial P}{\partial \eta} + \nabla^2 v, \tag{18}$$

$$PrRe\left[\frac{\partial T}{\partial t} - \frac{\eta}{g}\frac{\partial g}{\partial t}\frac{\partial T}{\partial \eta} + \frac{1}{\xi}\frac{\partial \xi uT}{\partial \xi} - \eta\frac{g'}{g}\frac{\partial uT}{\partial \eta} + \frac{1}{g}\frac{\partial vT}{\partial \eta}\right] = \nabla^2 T, \tag{19}$$

$$\nabla^2 = \frac{1}{\xi}\frac{\partial}{\partial \xi}\left(\xi\frac{\partial}{\partial \xi}\right) - \frac{2\eta g'}{g}\frac{\partial^2}{\partial \eta \partial \xi} + \left[2\left(\frac{g'}{g}\right)^2 - \frac{g''}{g} - \frac{g'}{g\xi}\right]\eta\frac{\partial}{\partial \eta} + \left[\left(\frac{g'\eta}{g}\right)^2 + \frac{1}{g^2}\right]\frac{\partial^2}{\partial \eta^2}. \tag{20}$$

The transformed boundary conditions become

$$\text{At } \xi = 0.1, \quad T = 1, \quad u = 0, \quad v = 0, \tag{21}$$

$$\text{At } \xi = 1, \quad T = 0, \quad u = 0, \quad v = 0, \tag{22}$$

$$\text{At } \eta = 0, \quad \frac{\partial T}{\partial \eta} = 0, \quad u = 0, \quad v = 0. \tag{23}$$

At the interface($\eta = 1$),

$$\frac{1+g'^2}{g}\frac{\partial T}{\partial \eta} - g'\frac{\partial T}{\partial \xi} = -NBiT, \tag{24}$$

$$v = \frac{\partial g}{\partial t} + g'u, \tag{25}$$

$$\left(\frac{1+g'^2}{g}\right)\frac{\partial u}{\partial \eta} - 2g'\frac{\partial u}{\partial \xi} + \left(\frac{g'+g'^3}{h}\right)\frac{\partial v}{\partial \eta} + (1-g'^2)\frac{\partial v}{\partial \xi} = -N\frac{\partial T}{\partial \xi}, \tag{26}$$

$$-P + \frac{2}{g}\left(\frac{\partial v}{\partial \eta} - g'\frac{\partial u}{\partial \eta}\right) + \frac{2g'}{N^2}\left(g'\frac{\partial u}{\partial \xi} - \frac{\partial v}{\partial \xi}\right) = \frac{1-CaT}{CaN}\left(\frac{g''}{N^2} + \frac{g'}{\xi}\right), \tag{27}$$

as in Eq. (11), P contains a free integration constant, $c(t)$. $g(t,r)$ and $c(t)$ are determined by Eqs. (27), (12), (13). A shooting method is used to find $c(t)$ at each time.

The free-surface shape, $g(t,r)$, is unknown and should be obtained as a solution of the coupled governing equations along with the surface force balance. The transformed governing Eqs. (16)–(19) and boundary conditions Eqs. (21)–(27), are solved by a finite volume method employing a SIMPLER algorithm. Nonuniform grids are constructed with finer meshes in the regions under the free surface and near the bottom and side walls where boundary layers develop. All computations are started with $g = 1$, $\mathbf{v} = 0$ and conduction temperature distribution. A brief summary of the computational procedure is as follows:

1. Start with initial conditions for T, $\mathbf{v}$, and g.
2. The rectangular computational domain is generated numerically.
3. Solve the transformed governing equations, Eqs. (16)–(19), to find T and $\mathbf{v}$ with the transformed boundary conditions, Eqs. (21)–(26).
4. Calculate g and c with the normal stress balance and liquid volume equations, Eqs. (27), (12), (13).
5. Steps (2)–(4) are repeated at each time step until all conditions for T, $\mathbf{v}$, and g are satisfied with the desired accuracy.
6. Return to step (1) for the next time step.

Convergence criteria for iterations within a time step or a steady state are $|s^{n+1} - s^n| < 10^{-9}$ and $|s^{n+1} - s^n|/|s^{n+1}| < 10^{-3}$, where s is any variable (u, v, T, g) at all points and n is time marching or iteration level. In addition, time histories of velocities and temperature at the mid-point of the free surface were compared to determine suitable time steps. In order to examine grid dependence, stream function minima are computed with various grids, Ca and V and listed in Table 1. A mesh of $71(r) \times 71(z)$ with nonuniform grids is used for all computations.

Table 1
Comparison of stream function minima with $Bi = 0$, where θ is a contact angle between the hot inside wall and the free surface

Re	V	Ca	Grid number ($r \times z$)	$\psi \times 10^2$
2000	1	0	61×61	−0.106
			71×71	−0.106
			91×91	−0.106
			121×121	−0.106
		0.05	61×61	−0.106
			71×71	−0.106
			81×81	−0.106
	0.817	0	61×61 ($\theta = 45$)	−0.209
			71×71 ($\theta = 45$)	−0.196
			81×81 ($\theta = 45$)	−0.190

The numerical code is validated by comparing computed surface temperatures with those from space experiments [16] in Fig. 2. The parameters for the simulation are $Pr = 97$, $Ar = 1(R_i/H = 0.111)$, $Ca = 0$ and $Re = 510$. Surface temperatures and gradients at the middle of the surface decrease with increasing Bi as shown in Fig. 2. The numerical results at $Bi = 2$ are in good agreement with experiments.

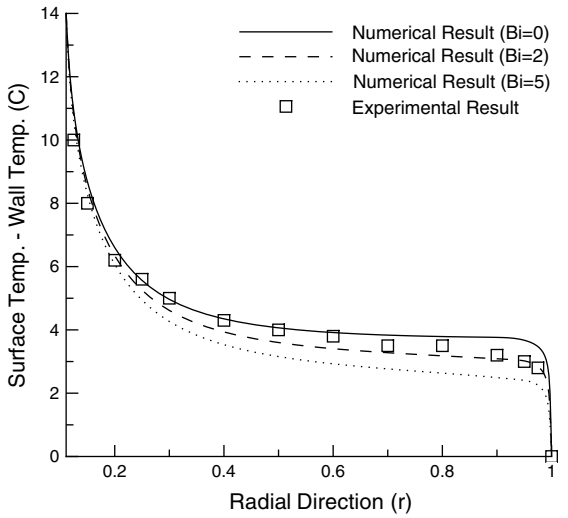

Fig. 2. Surface temperature distributions with $Pr = 97$, $V = 1$, $Ca = 0$, $Re = 510$ and $Ar = 1$ ($R_i/H = 0.111$). The numerical results with $Bi = 2$ are in good agreement with experiments [16].

4. Results and discussion

4.1. Effect of Re and Ca on thermocapillary convection with deformable surfaces and V = 1

We have investigated convection up to $Re = 5000$ with $Ca \leqslant 0.1$ and $Bi = 0$, and have found no axisymmetric oscillatory states with either nondeformable or deformable surfaces. In three-dimensional numerical simulations [17] with $Pr = 30$, $Ar = 1$, $Bi = 0$ and $Ca = 0$ (nondeformable flat surface), the critical Reynolds number for transition to oscillatory convection was about 2200. We thus conclude that dynamic free-surface deformations do not induce transition to unsteady, oscillatory convection, and only azimuthal waves can generate oscillations in this model. In addition, we have computed axisymmetric convection up to $Re = 10^4$ assuming undeformable and concave surfaces (see Section 4.1 below), and no unsteady, oscillatory convection was found. While oscillatory thermocapillary convection with a nondeformable surface in a rectangular cavity can be two-dimensional [18], it cannot be realized in an open annulus, an open cylinder ($Ar = 1$, $Pr = 30$) [14] with a uniform heat flux and a liquid bridge ($Ar = 0.714$, $Pr = 27$) [15]. We thus conclude that time-dependent, large Pr thermocapillary convection with the wavenumber of 0 does not occur in cylindrical geometries near $Ar = 1$.

Fig. 3 shows free surfaces with $Ca = 0.05$ and various Re. Curvature, sign and magnitude, is determined by both the surface pressure and normal viscous stresses as shown in Eq. (27). The surface is convex near the cold wall where surface pressure has a maximum positive value at the stagnation point, and concave near the hot wall. Two peaks appear at the free surface at sufficiently low Re, and the surface shape follows the surface pressure profile shown in Fig. 4 indicating small contribution from normal viscous stresses. As Re increases, viscous stresses dominate and cause additional ripples at the free surface which even becomes convex close to the hot corner. Surface elevations and depressions decrease with increasing Re due to this change in topology, volume conservation, and curvature.

Figs. 5 and 6 show the variations of the free surface with Ca at fixed $Re = 1$ and 2000, respectively. The shape of the surface, number of ripples, and reflection point do not change with Ca at a fixed Re, while the magnitudes of depressions and elevations increase with increasing Ca. Surface deformation is $O(10^{-4})$. Its maximum value is 1.2×10^{-3}, about 0.12% of the cylinder height, with $Re = 1$ and $Ca = 0.1$. The effect of Ca on stream function (ψ) minima, and surface temperature and velocity distributions is shown in Fig. 7. All are independent of Ca. Thus, dynamic surface deformations with $Ca \leqslant 0.1$ have little effect on the convection. This result is consistent with that from liquid bridges [11].

Fig. 8 shows the effect of Bi on the free surface with $Ca = 0.05$, $Re = 2000$. It derives from altered normal viscous stresses since the surface pressure is almost independent of Bi as shown in Fig. 9. The corresponding surface temperature and velocity distributions are shown in Fig. 10. While the magnitudes of the surface depressions and elevations change a little with Bi at fixed Re and Ca, the shape of the surface and the number of

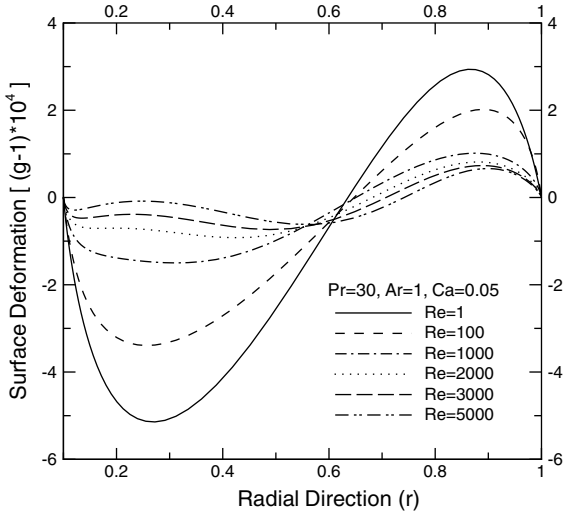

Fig. 3. Free surface deformations with $V = 1$, $Bi = 0$, $Ca = 0.05$ and various Re. Two free surface peaks increase to four with increasing Re.

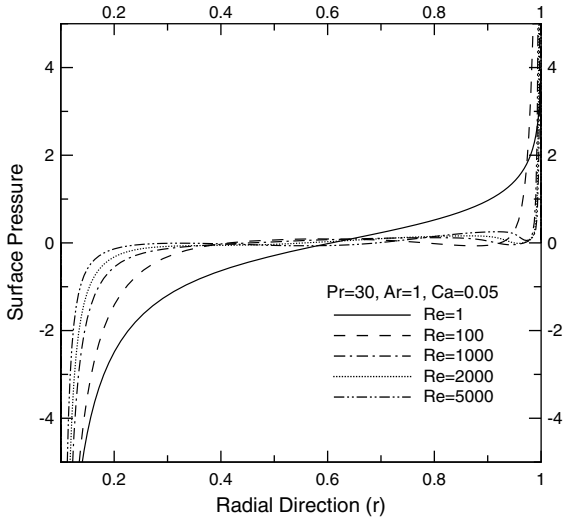

Fig. 4. Surface pressure distribution associated with Fig. 3. Surface curvature correlates with pressure at low Re.

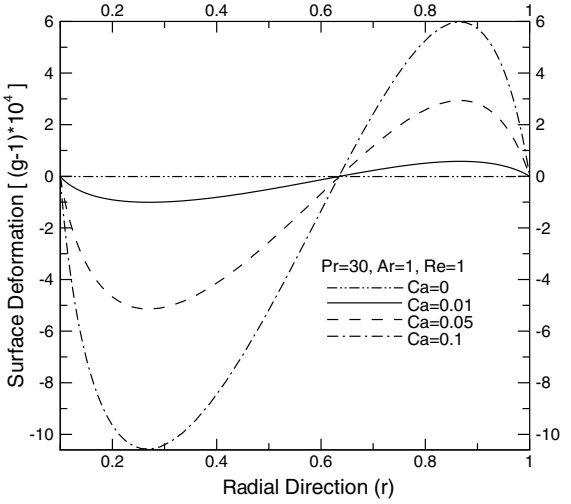

Fig. 5. Free surface deformation with $V = 1$, $Bi = 0$, $Re = 1$ and various Ca. The number of ripple and reflection point remain unchanged, while the magnitudes of depressions and elevations increase with Ca.

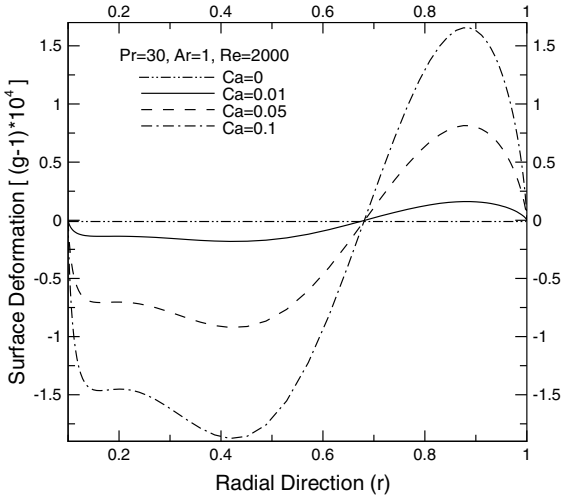

Fig. 6. Similar to Fig. 5 but with $Re = 2000$. Surface depressions and elevations are significantly smaller than those with $Re = 1$.

ripples do not change as shown in Fig. 8. Sharper temperature gradients develop at the hot corner with increased heat loss. This influences the thermocapillary force and hence surface deformation. Surface temperatures decrease with increasing Bi while surface velocities increase due to increased temperature gradient. Table 2 lists stream function minima with various Bi and Ca. Ca at fixed Bi has little effect on the convection as shown in Table 2 and Fig. 7, while Bi substantially influences the convection at fixed Ca.

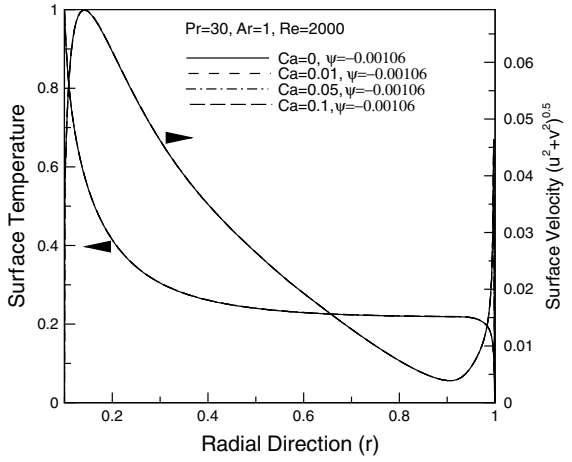

Fig. 7. Surface temperature and velocity distributions with $V = 1$, $Bi = 0$, $Re = 2000$ and various Ca. The deformable surface with $Ca \leq 0.1$ has little effect on the convection.

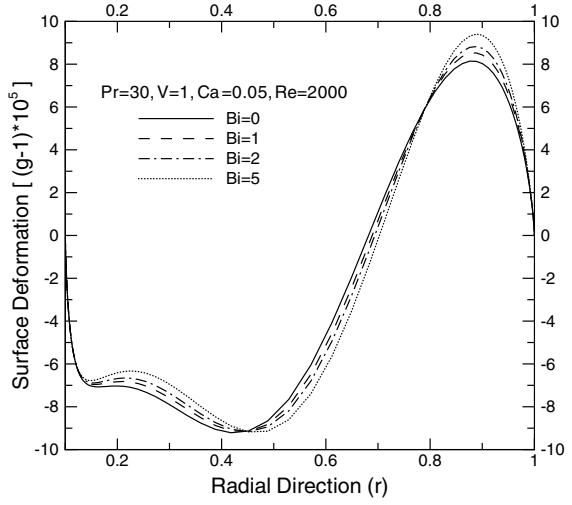

Fig. 8. Effect of heat loss on surface deformation with $V = 1$, $Ca = 0.05$ and $Re = 2000$.

4.2. Effect of free surface shape on thermocapillary convection with $Ca = 0$

In this section the free surface is nondeformable. At small Ca, the dynamic deviation of the surface shape from the static meniscus is negligible as shown in Figs. 5 and 6. With $Ca = 0$ the normal stress balance, Eq. (11), simplifies to the Young–Laplace equation and the free surface profile $g(r)$ obeys:

$$-Ca\Delta P = \frac{1}{N}\left(\frac{g''}{N^2} + \frac{g'}{r}\right), \tag{28}$$

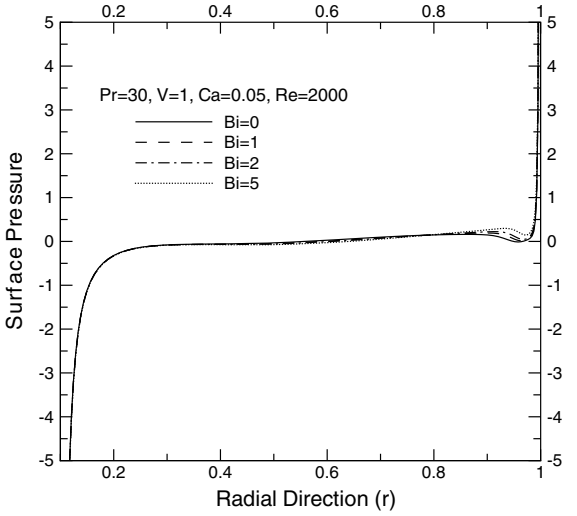

Fig. 9. Surface pressure corresponding to Fig. 8. It is almost independent of *Bi*.

where ΔP is the nondimensional pressure difference between the free surface and surroundings. The boundary conditions for Eq. (28) considered here are:

$$g'(0.1) = -\cot(\theta),$$

$$g(1) = 1, \qquad (29)$$

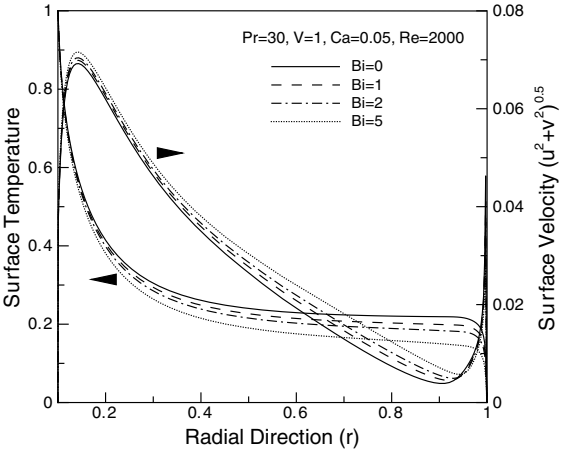

Fig. 10. Surface temperature and velocity distributions corresponding to Fig. 8. Larger hot corner temperature gradients at higher *Bi* drive faster surface flows.

Table 2
Stream function minima ($\psi \times 10^2$) with *Bi* at a fixed *Re* = 2000 and *V* = 1

Bi	*Ca* = 0	*Ca* = 0.05
0	−0.106	−0.106
1	−0.112	−0.112
2	−0.116	−0.116
5	−0.123	−0.123

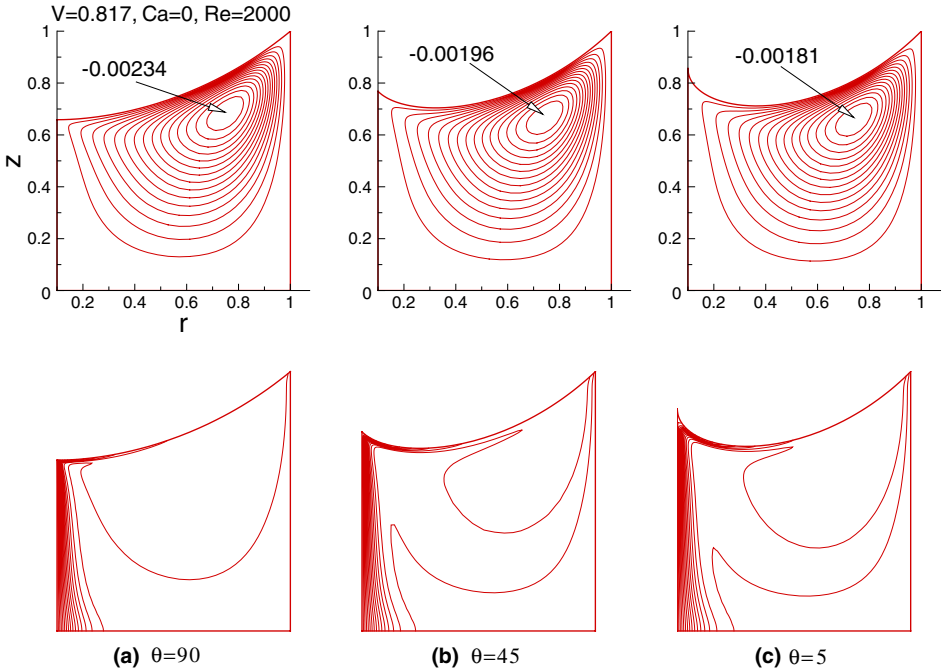

Fig. 11. Streamlines and isotherms with *Bi* = 0, *V* = 0.817, *Ca* = 0, *Re* = 2000 and (a) $\theta = 90$, (b) $\theta = 45$ and (c) $\theta = 5$. Convection is weakened with decreasing θ.

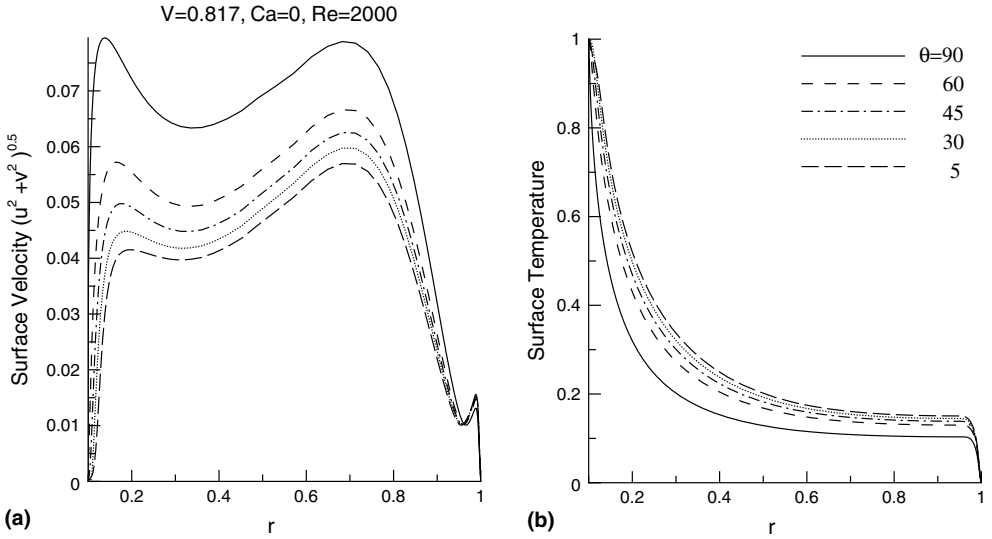

Fig. 12. Surface (a) velocity and (b) temperature distributions with various θ, $Bi = 0$, $V = 0.817$, $Ca = 0$ and $Re = 2000$. Velocity peaks increase and central temperatures decrease with increasing θ.

where θ is the hot corner contact angle. With a prescribed V and θ, $g(r)$ is determined by Eqs. (28) and (13) with boundary conditions, Eq. (29). In space experiments with a $Pr = 30$ liquid in a concave open annulus [3], θ was about 5°.

Convective flows with different θ at a fixed liquid volume ($V = 0.817$) and $Re = 2000$ are shown in Fig. 11. The corresponding surface velocity and temperature distributions are shown in Fig. 12. The flow fields show a large toroidal cell (without a secondary vortex) which is a characteristic of steady thermocapillary convection.

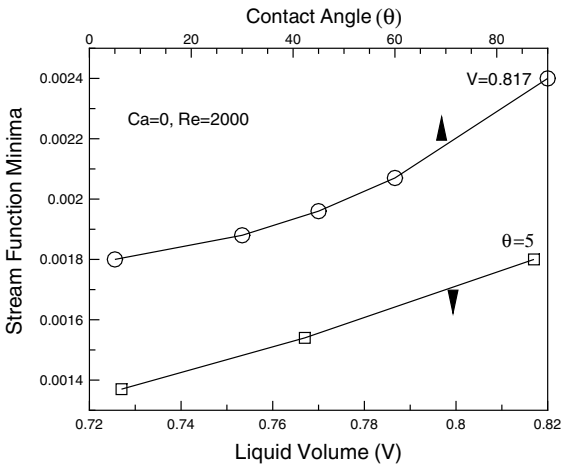

Fig. 13. Effects of (a) liquid volume and (b) contact angle on stream function minima with $Bi = 0$, $Ca = 0$ and $Re = 2000$. Convection is stronger with increasing V/θ at fixed $\theta = 5/V = 0.817$.

Surface temperatures near the middle of the free surface decrease with increasing θ, while surface velocities increase due to increased local surface temperature gradients and decreased local surface curvatures as shown in Fig. 12. Hence, convection is more vigorous with increasing V/θ at fixed θ/V as shown in Fig. 13. This result is consistent with space experiments [3], where the strength of convection increased with increasing liquid volume at a fixed Re and $\theta = 5$.

5. Conclusions

Axisymmetric thermocapillary convection in an open cylindrical annulus heated from the inside wall is computed. The deformable free surface, with pinned contact points, is obtained as a solution of the coupled transport equations and boundary conditions. Only steady convection is possible at any Re in this two-dimensional model with either nondeformable or deformable surfaces. Thus dynamic free surface deformations do not induce transitions to oscillatory axisymmetric convection even at large Re and Ca. Free surfaces are convex near the cold wall and concave at the hot wall. There are two peaks at low Re and more surface ripples at larger Re. The shape of the surface is independent of Ca at a fixed Re while the magnitudes of elevations and depressions increase with Ca. Heat loss from the surface substantially influences the dynamics with more vigorous convection at larger Bi. Convection depends significantly on free surface curvature. Computations with nondeformable concave interfaces ($Ca = 0$) at various V and θ indicate stronger circulations with increasing V/θ at fixed θ/V.

Acknowledgments

This work was supported by the Brain Korea 21 Project in 2002. We gratefully acknowledge the support of BK 21 and computer resources from the Rutgers Computational Grid composed of a Distributed Linux PC Cluster on which all computations were performed.

References

[1] D. Schwabe, U. Moller, J. Schneider, A. Scharmann, Instabilities of shallow dynamic thermocapillary liquid layers, Phys. Fluids 4 (1992) 2368–2381.
[2] D. Schwabe, Microgravity experiments on thermocapillary flow phenomena: Examples and perspectives, J. Jpn. Soc. Microgravity Appl. 16 (1999) 1–6.
[3] Y. Kamotani, S. Ostrach, J. Masud, Microgravity experiments and analysis of oscillatory thermocapillary flows in cylindrical containers, J. Fluid Mech. 410 (2000) 211–233.
[4] J. Chen, J. Sheu, S. Jwu, Numerical computation of thermocapillary convection in a rectangular cavity, Numer. Heat Tr. A 17 (1990) 287–308.
[5] J. Chen, F. Hwu, Oscillatory thermocapillary flow in a rectangular cavity, Int. J. Heat Mass Tr. 36 (15) (1993) 3743–3749.
[6] M. Hamed, J. Floryan, Marangoni convection. Part 1. A cavity with differentially heated sidewalls, J. Fluid Mech. 405 (2000) 79–110.
[7] Y. Jiang, H. Badr, J. Floryan, Thermocapillary convection with moving contact points, Phys. Fluids 15 (2003) 442–454.
[8] M. Mundrane, J. Xu, A. Zebib, Thermocapillary convection in a rectangular cavity with a deformable interface, Adv. Space Res. 16 (7) (1995) 41–53.
[9] M. Mundrane, A. Zebib, Low Prandtl number Marangoni convection with a deformable interface, AIAA J. Thermophys. Heat Tr. 9 (1995) 795–797.
[10] H. Kuhlman, C. Nienhuser, Dynamic free-surface deformations in thermocapillary liquid bridges, Fluid Dyn. Res. 31 (2002) 103–127.
[11] B.-C. Sim, W.-S. Kim, A. Zebib, Dynamic free-surface deformations in axisymmetric liquid bridges, Adv. Space Res., in press.
[12] M. Lappa, R. Savino, R. Monti, Three-dimensional numerical simulation of Marangoni instabilities in noncylindrical liquid bridges in microgravity, Int. J. Heat Mass Tr. 44 (2001) 1983–2003.
[13] M. Lappa, S. Yasushiro, N. Imaishi, 3D numerical simulation of on ground Marangoni flow instabilities in liquid bridges of low Prandtl number fluid, Int. J. Num. Meth. Fluids 13 (2003) 309–340.
[14] B.-C. Sim, A. Zebib, Thermocapillary convection with undeformable curved surfaces in open cylinders, Int. J. Heat Mass Tr. 45 (25) (2002) 4983–4994.
[15] B.-C. Sim, A. Zebib, Thermocapillary convection with undeformable curved surfaces in liquid bridges, AIAA J. Thermophys. Heat Tr. 16 (2002) 553–561.
[16] Y. Kamotani, S. Ostrach, A. Pline, A thermocapillary convection experiment in microgravity, J. Heat Tr. 117 (1995) 611–618.
[17] B.-C. Sim, A. Zebib, Effect of surface heat loss and rotation on transition to oscillatory thermocapillary convection, Phys. Fluids 14 (2002) 225–231.
[18] J. Xu, A. Zebib, Oscillatory two- and three-dimensional thermocapillary convection, J. Fluid Mech. 364 (1998) 187–209.